

# Nanoscale colloidal metals and alloys stabilized by solvents and surfactants

## Preparation and use as catalyst precursors<sup>1,2</sup>

H. Bönemann<sup>\*</sup>, G. Braun, W. Brijoux, R. Brinkmann, A. Schulze Tilling, K. Seevogel,  
K. Siepen

*Max-Planck-Institut für Kohlenforschung, D-45466 Mülheim a.d. Ruhr, Germany*

Received 12 February 1996

### Abstract

Solvent-stabilized organosols of the early transition metal series, e.g. Ti, Zr, Nb, and Mn, may be prepared by the reduction of the THF adducts or thioether solutions of the corresponding metal halides with  $K[BEt_3H]$ . Mono- and bimetallic organosols of Group 6–11 metals stabilized by tetraalkylammonium halides may be formed either by the reduction of the metal salts using  $NR_4$  hydrotriorganoborates or conventional agents, e.g.  $H_2$  or  $HCO_2H$ , after the pretreatment of the metal salts with  $NR_4X$ . The chemical reduction of transition metal salts in the presence of hydrophilic surfactants provides straightforward access to nanostructured mono- and bimetallic hydrosols. This synthesis can be performed even in water. Mono- and bimetallic nanoparticles stabilized by lipophilic or hydrophilic surfactants of the cationic, anionic or nonionic type serve as precursors for heterogeneous metal colloid catalysts effective for the hydrogenation and oxidation of organic substrates. Bimetallic precursors, e.g. Pt–Rh, have a synergic effect on the catalytic activity. A comparison of catalytic results and CO chemisorption experiments has revealed that the protecting surfactants still cover the nanoparticle surface after adsorption on supports, which markedly improves the lifetime of the catalysts. Chiral protecting agents may induce enantioselectivity in metal colloid catalysts.

*Keywords:* Metal colloids; Catalysis; Enantioselectivity

### 1. Introduction

Owing to their potential in surface chemistry, catalysis, and electronic microdevices, colloidal mono- and bimetallic materials have, after a period of hibernation, recently attracted more attention [1]. After physicists had provided most powerful analytical tools, which for the first time allowed the comprehensive characterization of these materials, the knowledge about nanoscale metal colloids has developed almost explosively, notably through chemical contributions made by Bouton-

net and coworkers [2,3], Bradley and coworkers [4–6], Braunstein [7], Esumi and coworkers [8–11], Evans and coworkers [12–14], Heaton [15], Henglein [16], Klabunde and coworkers [17–20], Knözinger [21], Larpent and Patin [22], Lewis and coworkers [23–26], Moiseev and coworkers [27,28], Schmid and coworkers [29–33], and Toshima and coworkers [34–38]. Some key publications of the field have been collected here [2–61]. An important advance consisted in the preparation of water-soluble nanoclusters using hydrophilic P or N donors as stabilizers [62–66].

Miscellaneous agents have been used for this purpose [34,35,67–80]. The first nanoscale metals stabilized by surfactants were reported in 1976 by Lisichkin et al. [81] and 1979 by Kiwi and Grätzel [82]. The object of this paper is to summarize some chemical reduction pathways to nanoscale metal and metal alloy colloids utilizing either surfactants or solvents as the stabilizing

<sup>\*</sup> Corresponding author.

<sup>1</sup> Based on a lecture held at the 5th Königstein–Kreuth Conference, Wildbad–Kreuth, Germany, October 3–6, 1995.

<sup>2</sup> Dedicated to the memory of H. Takaya.

Ti	V	Cr	Mn	Fe	Co	Ni	Cu	Zn
Zr	Nb	Mo		Ru	Rh	Pd	Ag	
Hf	Ta	W	Re	Os	Ir	Pt	Au	Hg

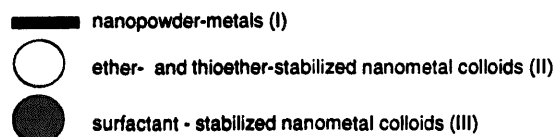
- 
  
 ■ nanopowder-metals (I)
   
 ○ ether- and thioether-stabilized nanometal colloids (II)
   
 ● surfactant-stabilized nanometal colloids (III)

Fig. 1. Survey of powder or colloidal nanometals.

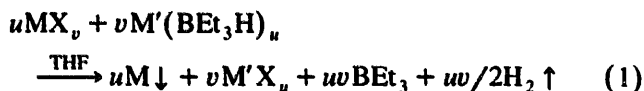
agents. In addition, the application of these nanostructured materials as precursors for a new type of catalyst will be discussed. In the course of our research in this area, we have developed various methods for the preparation of stable and very soluble metal organo- and hydrosols having a narrow particle size distribution. The metallic core derived from elements of Group 6–11 is protected either by lipophilic or hydrophilic surfactant molecules [34,83–91]. Recently, Reetz and coworkers have found an alternative electrochemical access to this class of nanoparticles [92–94]. In the early transition metal series, e.g. Ti, Zr, Nb, and Mn, the stabilization is achieved by THF or the corresponding thioether to give very soluble organosols [95,96] (Fig. 1).

The reduction of transition metal salts and oxides using alkali hydrotriorganoborates in organic media in the absence of stabilizers at ambient temperature leads to X-ray amorphous nanopowders of metals and alloys [97]. In contrast, the reduction of ether and thioether adducts of early transition metal halides, with  $K[BEt_3H]$ , gives isolable organosols of zerovalent Ti, Zr, V, Nb, and Mn stabilized by ether or thioether molecules respectively. The use of tetraalkylammonium hydrotriorganoborates as reducing agents leads to mono- and bimetallic organosols. Pretreatment of transition metal halides with various hydrophilic surfactant types prior to the reduction using conventional agents, e.g.  $H_2$  or  $HCO_2H$ , provides easy access to nanostructured mono- and bimetallic hydrosols of Group 8–11 metals. This synthesis can be performed even in water. Mono- and bimetallic hydrosols of this type serve as effective precursors for heterogeneous metal catalysts for the selective hydrogenation and oxidation of organic substrates. Electron microscopy has revealed that these colloidal metal systems stabilized either by surfactants or solvents are very monodisperse and may be deposited onto supports without any unwanted agglomeration. This is a major prerequisite for size selective studies in heterogeneous catalysis [83,84,87,98].

## 2. Results and discussion

### 2.1. X-ray amorphous metal nanopowders

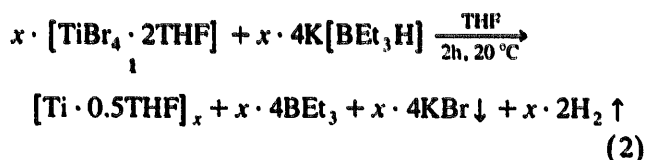
Metal salts of Group 6–12 and  $SnCl_2$  may be reduced using alkali hydrotriorganoborates in hydrocarbons between  $-20\text{ }^\circ\text{C}$  and  $80\text{ }^\circ\text{C}$  to give boron-free powdery metals. According to X-ray diffraction the particles are nearly amorphous. The particle size of the powders according to transmission electron microscopy (TEM) is between 1 and 100 nm, dependent on the metal (Fig. 2). By simple coreduction of suspended metal salts binary or ternary alloys and intermetallic compounds were obtained [97].



X = halogen

### 2.2. Ether-stabilized organosols of $Ti(0)$ , $Zr(0)$ , $V(0)$ , $Nb(0)$ , and $Mn(0)$

The reduction of  $TiCl_4 \cdot 2THF$  or  $TiCl_3 \cdot 3THF$  in THF with  $K[BEt_3H]$  gives colloidal titanium stabilized by THF. After evaporating the solvent and  $BEt_3$  and thoroughly drying in vacuo a black pyrophoric powder (containing small amounts of KCl) is obtained. Protonolysis and cross-experiments using  $K[BEt_3D]$  as the reducing agent indicated the presence of residual hydrogen in the resulting Ti colloid [95,96]. In contrast, the reduction of  $TiBr_4 \cdot 2THF$  1 according to Eq. (2) yields a hydrogen-free colloidal  $[Ti \cdot 0.5THF]_x$  2 consisting of 44% Ti and 1% KBr.



No particles were detected by high resolution (HR)TEM, indicating that the size is less than 0.8 nm. The careful analytical examination of the electronic and geometric structure of this extremely oxyphilic Ti

Cr	Mn	Fe	Co	Ni	Cu	Zn		
			3–5 nm	5–15 nm	25–90 nm			
		Ru	Rh	Pd	Ag	Cd	Sn	
		1–4 nm	12–20 nm					
	Re	Os	Ir	Pt	Au			
			2–5 nm					

Fig. 2. X-ray amorphous nanopowders and alloys.

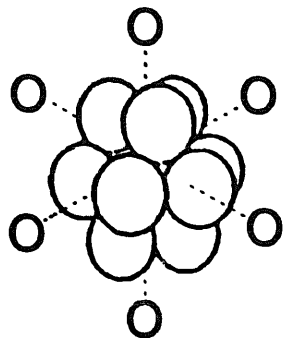
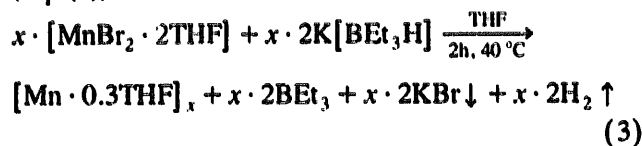


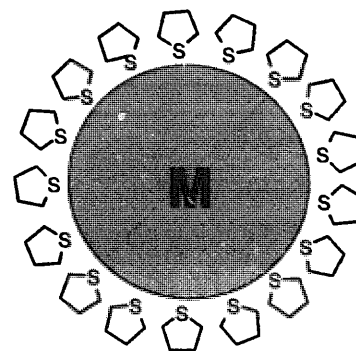
Fig. 3. Regular  $Ti_{13}^0$  cluster having six THF-O atoms in an octahedral configuration.

organosol **2** by means of IR spectroscopy, X-ray diffraction, X-ray photoelectron spectroscopy (XPS), X-ray absorption near-edge structure (XANES), and extended X-ray absorption fine structure (EXAFS) [95,96] revealed that **2** consists of very small Ti particles in the zerovalent state stabilized by intact THF molecules. The EXAFS spectra showed signals at 1.6 Å and 2.4 Å; no signals from backscatterers greater than 3 Å were observed. The Ti–Ti distance found (2.804 Å) was smaller than in the bulk Ti metal and the Ti–O distance was 1.964 Å. On the basis of these findings **2** is best described as a regular  $Ti_{13}$  cluster having six THF-O atoms in an octahedral configuration (Fig. 3).

Analogously, the corresponding Zr colloid may be isolated; on the slow addition of the filtered THF solution slowly to pentane (removal of residual KCl) the Zr colloid precipitates. The workup of the V and Nb colloids is performed similarly. The reduction of the THF adduct to  $MnBr_2$  at 40 °C yielded a stable, isolated  $[Mn \cdot 0.3 THF]_x$  colloid containing typically 60% Mn (Eq. (3)).



IR and NMR data of the colloid show intact THF coordinated to Mn. HRTEM shows the fringes of Mn particles of the size 1–2.5 nm. No bromine was detectable by energy-dispersive X-ray (EDX) analysis of the Mn nanoparticles and XANES and EXAFS con-



M = Ti, V (decomposition)

M = Mn, Pd, Pt stable organosols

Fig. 4. Organosols stabilized by tetrahydrothiophene.

firmed that colloidal Mn(0) was formed according to Eq. (3) [88]. Table 1 summarizes the results achieved so far with THF-stabilized organosols of early transition metals [99,100].

The colloidal stabilization of zerovalent nanometals may also be achieved using tetrahydrothiophene as the donor molecule in a synthesis similar to Eq. (3). In the case of Mn, Pd and Pt, stable organosols were isolated; however, sols of Ti and V quickly decomposed (Fig. 4).

### 2.3. Organosols via the stabilization of nanometals by lipophilic surfactants

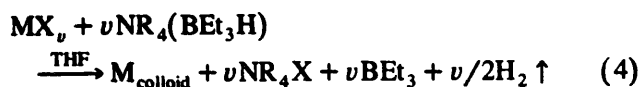
Lipophilic surfactants of the cationic type such as tetraalkylammonium halides have been used previously by various workers, e.g. see Refs. [2,3,2,81,82], as highly efficient protecting groups for nanometals giving very stable organosols, isolable in the form of dry powders containing up to 85 wt.% of metal [83,87,89,98]. The reduction of suspended metal salts using tetraalkylammonium hydrotriorganoborates in organic solvents (see Eq. (4)) occurs very smoothly giving metal organosols stabilized by  $NR_4^+$  [82] which is present at the reduction center in a high local concentration. The metal particles (1–10 nm in size) are well protected from agglomeration by the long-chain alkyl groups so that very little metal (if any) precipitates. This

Table 1  
THF-stabilized organosols of early transition metals

Product <sup>a</sup>	Starting material	Reducing agent	T(°C)	t (h)	Metal content (%)	Size (nm)
$[Ti \cdot 0.5THF]_x$	$TiBr_4 \cdot 2THF$	$K[BEt_3H]$	rt	6	43.5	(< 0.8)
$[Zr \cdot 0.4THF]_x$	$ZrBr_4 \cdot 2THF$	$K[BEt_3H]$	rt	6	42	–
$[V \cdot 0.3THF]_x$	$VBr_3 \cdot 3THF$	$K[BEt_3H]$	rt	2	51	–
$[Nb \cdot 0.3THF]_x$	$NbCl_4 \cdot 2THF$	$K[BEt_3H]$	rt	4	48	–
$[Mn \cdot 0.3THF]_x$	$MnBr_2 \cdot 2THF$	$K[BEt_3H]$	50	3	70	1–2.5

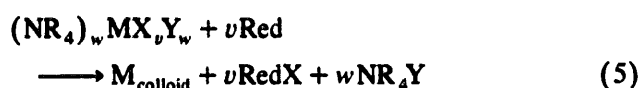
<sup>a</sup> For details see Section 7.1.1.

very lipophilic type of surfactant makes the resulting organosols very soluble in organic phases so that up to 1 M metal solutions are easily obtainable.



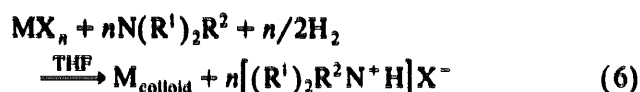
M = metals of Groups 6–11; X = Cl, Br;  $v = 1, 2, 3$ ; R = alkyl,  $\text{C}_6\text{--}\text{C}_{20}$

The necessary pre-preparation of the alkylammonium organoborate (Eq. (4)) can be avoided by coupling the  $\text{NR}_4\text{X}$  agent to the metal salt prior to the reduction step. This again provides a high local concentration of the protecting agent right at the reduction center so that the reduction itself may now be performed using a large variety of conventional inorganic or organic reducing agents (Eq. (5)).



M = metals; Red =  $\text{H}_2$ ,  $\text{HCOOH}$ , K, Zn, LiH,  $\text{LiBEt}_3\text{H}$ ,  $\text{NaBEt}_3\text{H}$ ,  $\text{KBEt}_3\text{H}$ ; X, Y = Cl, Br;  $v, w = 1\text{--}3$ ; R = alkyl,  $\text{C}_6\text{--}\text{C}_{12}$

In the case of noble metals the simple reduction of the THF suspended metal salts using  $\text{H}_2$  in the presence of trialkylamines proved to be an effective and clean synthetic alternative (Table 2). This pathway avoids the formation of alkali salt byproducts completely (Eq. (6)).

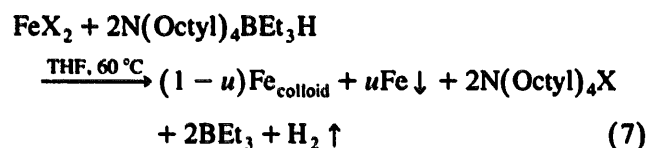


M = Ru, Rh, Pt  
 X = Cl, Br  
 $\text{R}^1 = \text{C}_8\text{H}_{17}$   
 $\text{R}^2 = \text{CH}_3, \text{C}_8\text{H}_{17}$   
 Ru:  $60^\circ\text{C}$ , 1–50 bar  $\text{H}_2$ , 24 h  
 Rh:  $60^\circ\text{C}$ , 1–50 bar  $\text{H}_2$ , 16 h  
 Pt:  $20^\circ\text{C}$ , 1 bar  $\text{H}_2$ , 1 h

Comparing the utility of the three synthetic alternatives given in Eqs. (4)–(6) it can be stated that the ‘ammonium borate method’ (Eq. (4)), using a powerful

reducing agent, provides the most general access to mono- and bimetallic organosols via the reduction or coreduction of metal salts between Group 6 and 11 PSE. The ‘double-salt method’ (Eq. (5)), in contrast, provides an easy access to these materials; however, Group 6 metal organosols and colloidal Fe(0) cannot be produced in this way. The amine variation described in (Eq. (6)), where the protective ammonium group is formed via ‘self-construction’ at the particle surface during the reduction step, is certainly the cleanest access to metal organosols; however, its application appears to be limited to noble metal salts which are easy to reduce.

Interestingly, Fe(0) organosols turned out to be the most difficult example to prepare in the Group 6–11 transition metal series. Using the ‘ammonium borate method’ (Eq. (4)) no reduction of e.g.  $\text{FeBr}_2$  occurs at  $25^\circ\text{C}$  even after 10 days of stirring. At  $60^\circ\text{C}$ , however, the salt suspended in THF dissolves completely within 24 h. During the evolution of hydrogen ca. 50% of the Fe precipitates as a magnetic powder, which is removed by filtration (Eq. (7)).



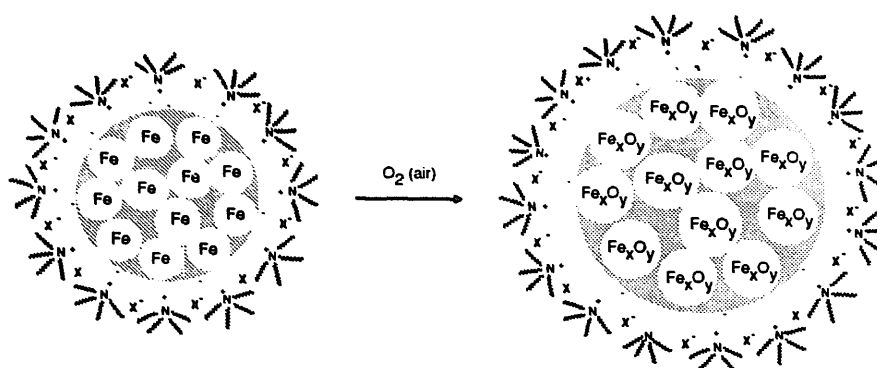
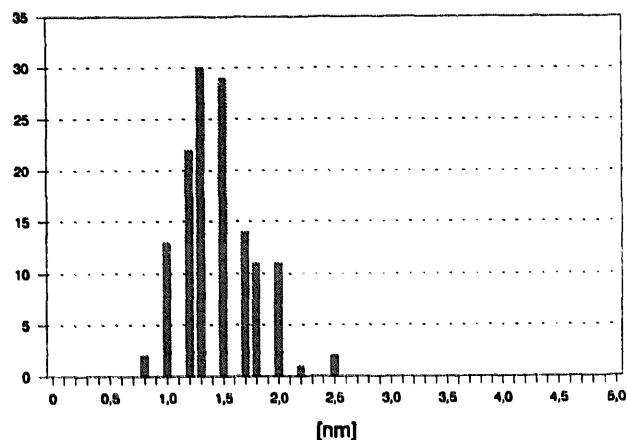
X = Br, I

Subsequent workup of the reddish-black colloidal Fe solution and further purification of the raw product by precipitation of the redispersed material in THF by slow addition of pentane to the solution gave the dry organosol (particle size 3 nm) containing 14% of Fe(0) (oxidation state evident from Mössbauer spectra), which proved to be fully redispersible in THF and toluene [99]. This nanosized colloidal Fe is extremely oxyphilic both in solution and in powder form. On the carefully controlled addition of air (16 h), however, the dissolved  $\text{N}(\text{octyl})_4\text{Br}$ -stabilized Fe(0) organosol slowly oxidizes

Table 2  
Preparation of noble metal colloids by reduction using  $\text{H}_2$  in the presence of  $\text{N}(\text{octyl})_3$

No.	Metal salt	Conditions			Product colloid (solution colour)	Work up solvent	Solvent added for precipitation	Metal content in isolated colloid (%)	Mean particle size (nm)
		$\text{H}_2$ -pressure (bar)	t (h)	T ( $^\circ\text{C}$ )					
1	$\text{RuCl}_3 \cdot 3\text{H}_2\text{O}$	1–50	24	60	dark brown to black Ru completely dissolved	ethanol	pentane	75.5	1.1
2 <sup>a</sup>	$\text{RhCl}_3 \cdot 3\text{H}_2\text{O}$	1–50	16	60	dark brown to black Rh completely dissolved	ether	ether	60.99	2.4
3	$\text{PtCl}_2$	1	1	20	black Pt completely dissolved	–	–	–	2.9

<sup>a</sup> For details see Section 7.1.8.

Fig. 5. Oxidation of the  $\text{NR}_4^+$ -stabilized Fe colloid.Fig. 6. Particle size distribution of an  $\text{NR}_4^+$ -stabilized Ru colloid.

giving a rusty-brown solution of colloidal Fe oxide, which is stable in air for several days and may be kept under argon even for months without any sedimentation [101] (see Fig. 5).

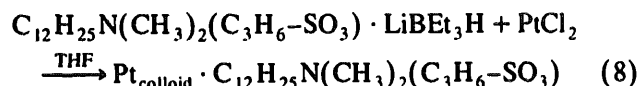
Since the synthesis pathways (Eqs. (4)–(6)) provide a high local concentration of the protecting agent right at the reduction center, the resulting colloid particles consequently are rather small and monodisperse. A typical particle size distribution histogram, derived from the electron micrograph, of a Ru organosol is shown in Fig. 6.

Fig. 7 summarizes the results obtained in the preparation of transition metal organosols stabilized by lipophilic  $\text{NR}_4^+$  surfactants as the protecting agent [89].

#### 2.4. Hydrosols via the stabilization of nanometals by hydrophilic surfactants

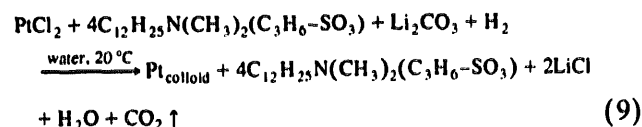
For the effective synthesis of stable nanometal hydrosols via chemical reduction we first tried to transfer the principle of combining the reduction agent with the protective group (used in Eq. (4) for the synthesis of organosols) to hydrophilic surfactants such as betaines. For example 3-(*N,N*-dimethyldodecylammonio)-pro-

panesulfonate (SB12) reacts in THF suspension with Li hydrotriorganoborate to form a strongly reducing THF-soluble 1:1 adduct [102], the structure of which is currently under investigation. This adduct was used to reduce a number of transition metals salts of Groups 8–11 PSE in THF to give mono- and bimetallic hydrosols, which precipitate from THF. The resulting nanometallic materials (particle size 1–6 nm) proved to be highly soluble in water. An example of this new synthesis of transition metal hydrosols is given in (Eq. 8).



The zerovalent state of the metal core was checked by X-ray absorption and XPS [103]. All analytical data obtained so far of the various sulfobetaine-stabilized nanometallic hydrosols are in full agreement with the schematic structure depicted in Fig. 8.

The method of coupling the stabilizing surfactant to the metal salt prior to reduction (analogous to Eq. (5)) allows the performing of metal hydrosol synthesis even in water. This variation (Eq. (9)) led us to highly water soluble colloidal nanometals (mono- and bimetallic), stabilized by hydrophilic surfactants of the anionic, nonionic or amphiphilic types, using e.g. hydrogen, Li formates or alkali borohydrides, as reducing agents in aqueous solution.



The consequent application of both synthetic pathways described in Eqs. (8) and (9) in our hands has made a plethora of mono- and bimetallic hydrosols accessible (see Table 3).

Since both the synthesis methods (Eqs. (8) and (9)) favor a high local concentration of the protecting agent at the reduction center, the resulting hydrosol particles are consequently found by TEM to be rather small

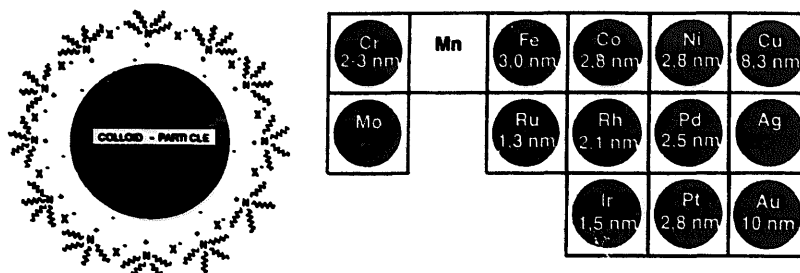


Fig. 7.  $\text{NR}_4^+$ -stabilized organosols and diameter of the metal core.

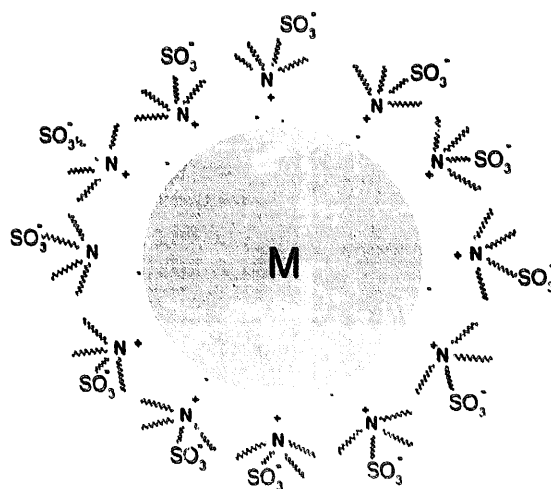
(1–10 nm). The electron micrographs also show a very narrow particle size distribution to be present in the hydrosols.

### 3. Nanometal powders from organosols

After the extraction of the protecting shell from the metal core of the colloid using e.g. ethanol, nanometal powders of the same particle size as the colloidal starting material may be obtained. For example, the extraction of colloidal Pt (mean particle size 2.8 nm) with ethanol yields a grey Pt powder of 2.8 nm size according to TEM [83].

During the physical characterization of the colloidal materials through electron microscopy (specifically EDX) and XPS, both of which employed ultra high vacuum conditions ( $10^{-7}$  to  $10^{-8}$  Pa), the nitrogen of the  $\text{NR}_4\text{X}$  groups could not be detected. This clearly indicates that the protecting tetraalkylammonium halide may be removed under certain conditions leaving the

bare metal core behind. This observation prompted us to develop a chemical procedure for the extraction of the protecting shell from the colloids at room temperature to produce nanoscale metal powders (given in Table 4). The preparation of nanoscale platinum powder from the corresponding platinum colloid represents a typical example. The grey-brown colloid powder is treated with an excess of ethanol, after which the supernatant solution containing the tetraalkylammonium halide is siphoned off. This procedure is repeated several times during which a continuous darkening of the product color is observed. The resulting black pyrophoric metal powder (93 wt% Pt) is no longer redispersible in THF (Table 4, No. 5). The TEM image of this product shows that the mean particle size of the platinum powder after the extraction corresponds exactly to that of the initial colloidal platinum sample. As determined by EDX analysis the extracted sample still contains traces of the protecting shell, which can be completely removed by heating the metal powder at 700 °C under vacuum (0.1 Pa). According to the TEM image of the heated product



M = Cu, Ru, Rh, Pd, Ag, Ir, Pt, Ru/Fe, Ru/Co, Ru/Ni, Ru/Cu, Pt/Co, Pt/Cu, Ru/Rh, Ru/Ir, Ru/Pt, Rh/Ir, Rh/Pt, Pd/Pt, Ir/Pt

Fig. 8. Sulfobetaine-stabilized colloidal metals and alloys.

the mean particle size is 2.8 nm, the same value found for the original colloidal platinum. Hence, an agglomeration of the metallic nanoparticles as a consequence of heat treatment is not observed.

This finding holds basically true in almost every preparation of metallic or intermetallic powder from the corresponding colloidal material (compare the particle sizes listed in Table 4). The only exception found so far

Table 3  
Stabilization of water-soluble colloids by various surfactant types

Surfactants	Metals
<p><b>Cationic type</b></p> $\text{C}_{18}\text{H}_{37}\text{N}^+\text{CH}_2\text{CH}(\text{OH})\text{CH}_2\text{Cl} \text{ Cl}^-$ <p style="text-align: center;"> <math>\begin{array}{c} \text{CH}_3 \\   \\ \text{N}^+ \\   \\ \text{CH}_3 \end{array}</math> </p> <p><i>QUAB 426</i></p> $(\text{R COCH}_2\text{CH}_2)_n \text{N}^+\text{CH}_3 (\text{CH}_2\text{CH}_2\text{OH})_{3-n}$ <p>R = partially hydrogenated C<sub>15</sub>-group</p> <p><i>ESTERQUAT AU35</i></p>	Pt
<p><b>Anionic type</b></p> $\text{RCNH}(\text{CH}_2)_n\text{N}^+\text{CH}_2\text{CO}_2\text{Na}$ <p style="text-align: center;"> <math>\begin{array}{c} \text{O} \\    \\ \text{CH}_2\text{CH}_2\text{OH} \end{array}</math> </p> <p>R = Cocoalkyl</p> <p>Na-Cocoamidoethyl-N-hydroxyethyl-glycinate <i>DEHYTON G</i></p>	Pt
<p><b>Nonionic type</b></p> <p>Polyoxyethylenelaurylether, <i>BRIJ 35</i><sup>a</sup></p> <p>Polyoxyethylenesorbitanmonolaurate, <i>TWEEN 20</i></p>	Co, Rh, Pt, Pt/Pd <sup>a</sup>
<p><b>Amphiphilic types</b></p> <p><b>Betaines</b></p> <p>3-(N,N-Dimethyldodecylammonio)-propanesulfonate (SB12)<sup>b</sup></p> <p>Lauryldimethylcarboxymethyl-ammoniobetaine, <i>REWO</i></p> <p>Cocoamidopropylbetaine, <i>DEHYTON K</i></p> <p>Coccamidopropylbetaine, <i>AMPHOLYT JB130</i></p> <p><b>Sugar derivatives</b></p> <p>Alkylpolyglycosides, <i>APG 600</i></p>	<p>Cu, Ru, Rh, Pd, Ag, Ir, Pt<sup>b</sup></p> <p>Ru/Fe, Pt/Co, Pt/Cu, Ru/Rh,</p> <p>Ru/Ir, Ru/Pt, Rh/Ir, Rh/Pt,</p> <p>Pd/Pt, Ir/Pt</p> <p>Pt</p>

involves palladium (Table 4, No. 4), where a particle growth from 2.5 to 5.8 nm is seen (via TEM) upon removing the protecting shell. After the thermal treatment no further particle growth is detected.

Precipitated nanopowders obtained by chemical reduction may be transferred into soluble metal colloids by subsequent reaction with  $\text{NR}_4\text{X}$ . For example, a sample of magnetic cobalt powder (particle size 4 nm), precipitated from  $\text{CoBr}_2$  by reduction in THF was reacted with an excess of  $\text{N}(\text{Octyl})_4\text{Br}$  to give a clear, dark red solution of the corresponding cobalt organosol.

#### 4. Colloidal alloyed metals

The coreduction of a mixture of different tetraalkylammonium metalates yields colloidal metal alloys. HRTEM of the product of the coreduction of  $(\text{NR}_4)_3\text{RhCl}_6$  and  $(\text{NR}_4)_2\text{PtCl}_4$  (magnification:  $6.3 \times 10^5$ ) showed particles of an average size of 2.3 nm and a net plane distance of 0.25 nm. Under the microscope, 70 particles were analyzed by EDX with a point resolution of 1 nm. In every particle examined, both Rh and Pt were found to be present, which indicates that in fact a colloidal Pt–Rh alloy is generated during coreduction. An EXAFS study of a  $\text{Pt}_{56}\text{Rh}_{44}$  colloid at both the Rh K-edge and the Pt L<sub>III</sub>-edge verified the formation of a bimetallic alloy nanoparticulate system [90]. In subsequent X-ray absorption spectroscopy studies, the structural characterization of a series of Pt–Rh colloids with varying stoichiometries was achieved. The results of these investigations together with electrochemical studies, XPS and X-ray diffraction measurements will be the subject of forthcoming papers [91].

#### 5. Catalytic applications

The goal behind the preparation of novel metal and alloy colloids includes, in addition to possible applica-

tions in the field of electronic 'nanodevices' [104], the development of promising new homogeneous and heterogeneous catalysts. The catalytic potential of the colloidal materials was explored both in the homogeneous phase and in the supported state. Regarding the former, the activities of a series of palladium colloids were measured for the hydrogenation of cyclohexene in THF under normalized conditions [84]. The catalytic activity as well as selectivity and long time stability of noble metal colloids adsorbed on charcoal, 5 wt.% Pd [85], 5 wt.% Rh [83] and 5 wt.% Pt [83], were tested in the hydrogenation of cinnamic acid, butyronitrile or crotonic acid respectively. Further, the selective oxidation of glucose giving gluconic acid using a bimetallic Pd–Pt colloid as the active component has been recently included in these studies. The experimental apparatus and the test conditions employed in the investigations of the heterogeneous charcoal supported catalysts are described in detail in Ref. [84].

##### 5.1. The precursor concept

Pre-prepared nanometals stabilized by surfactants may be used as easily accessible precursors for a new type of heterogeneous catalyst. These precursors may be optimized independent of the support by varying the particle size, the composition and structure of bimetallic systems. Further, the coverage of the metal surface by various protective shells and intermediate layers, e.g. oxygen or sulfur, may be used for modifications of the active component. This is visualized in Fig. 9.

Since modern analytical tools such as HRTEM, EDX, XPS, XANES, and EXAFS provide detailed physical data about the size, composition, oxidation state, and structure of the precursor particles, all prerequisites necessary for the 'molecular design' of catalyst precursors are given. The perfect protection of the nanometallic hydrosols by the various hydrophilic surfactants listed in Table 3 allows the handling of the precursors even in concentrated aqueous solution. Further, the use

Table 4  
Preparation of monoscale metal powders via metal colloids

No.	Starting material		Solvent for extraction of $\text{NR}_4\text{X}$	Product metal content after extraction (%)	Mean particle size	
	Colloid	Mean particle size (nm)			after extraction (nm)	after heat treatment (700 °C, 4 h, 0.1 Pa) (nm)
1	Co	2.8	ethanol	82.84	3.8	–
2	Ni	2.8	ethanol	88.18	3.0	–
3	Rh	2.1	ethanol	82.76	2.7	2.9
4	Pd	2.5	ethanol	98.13	5.8	6.0
5	Pt	2.8	ethanol	92.90	2.8	2.8
6	Rh–Pt	2.3	ether:ethanol 1:10	–	2.7	3.0
7	Pd–Pt	2.8	ether:ethanol 1:10	–	2.8	–



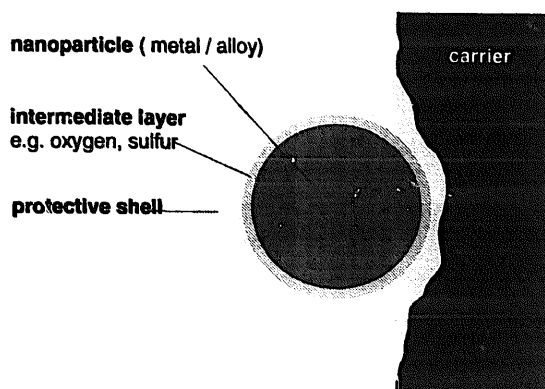


Fig. 9. The precursor concept.

of surfactants as the protective shell around the metal core enables the efficient adsorptive fixation of the metal particles, even on single crystalline oxides such as quartz, sapphire or on highly oriented pyrolytic graphite (HOPG), simply by dipping these substrates into aqueous solutions of the nanometal hydrosols at 20 °C. A combined atomic force microscopy (AFM), scanning tunneling microscopy (STM), and XPS study by Behm et al. [105] has further revealed that the supported metal particles are very resistant to agglomeration even under extreme conditions. For example, AFM of an alumina supported Pt SB12 hydrosol after annealing the sample in vacuo at 500 °C still showed individual, sphere-shaped Pt species randomly distributed over the support surface.

### 5.2. Heterogeneous catalysts on the basis of surfactant stabilized precursors

In order to prepare heterogeneous catalysts, the precursors may be adsorbed from aqueous solutions on the supports simply by dipping at ambient temperature. According to TEM no agglomeration of the particles occurs [83]. The advantage of supported colloid catalysts is demonstrated, e.g. by comparison of the activity of two Rh catalysts (5% Rh on charcoal), in the butyronitrile hydrogenation test (hydrogenation of butyronitrile to butylamine) (Fig. 10).

The electron micrograph of the conventional catalyst made by salt impregnation and subsequent calcination shows large metal agglomerations on the surface besides a minor fraction of Rh particles of 1–5 nm size. Using a Rh colloid precursor of 1.2–2.2 nm particle size on the same support the activity observed in the test reaction is virtually doubled. Both catalyst types show a significant increase of activity when doped with 0.2% of the Ti(O) colloid 2.

In addition, the lifetime of the colloid catalyst is superior to the conventional precipitation systems. Whereas the activity of a conventional Pd–C catalyst tested in the hydrogenation of cyclooctene to cyclooctane expires completely after the performance of  $38 \times 10^3$  catalytic cycles per Pd atom, the Pd colloid–C catalyst still shows a residual activity after  $96 \times 10^3$  catalytic turnovers (see Fig. 11).

Selectivity control may be brought about by doping

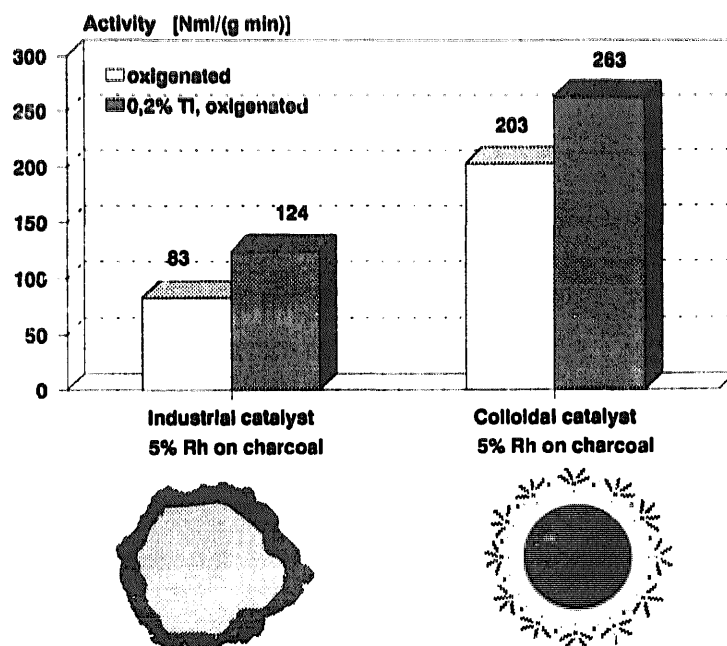


Fig. 10. Activity of Rh–C catalysts in the butyronitrile hydrogenation test.

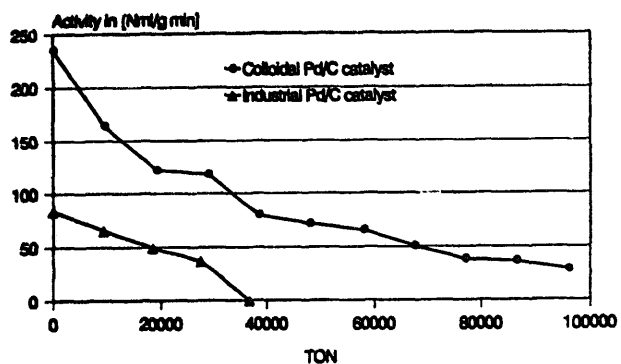


Fig. 11. Lifetime of Pd-C catalysts in the cyclooctene hydrogenation test.

by adding a second metal. For example, doping of Rh colloid catalysts with Sn has a strong effect on the selective C=O group hydrogenation of  $\alpha, \beta$ -unsaturated aldehydes.

A Rh colloid-C catalyst doped with Sn (Rh/Sn = 1.5/1) exhibits 86% selectivity in the hydrogenation of cinnamic acid to cinnamic alcohol [106]. Using the catalytic hydrogenation of crotonic acid to butanoic as a test reaction, we were able to observe the synergistic effect of bimetallic colloidal precursors (see Fig. 12) [83]. The catalysts prepared by mixing Pt colloid-C and Rh colloid-C powders or by consecutive adsorption of Pt and Rh colloid on charcoal show a linear increase of activity with increasing content of Rh (additive effect).

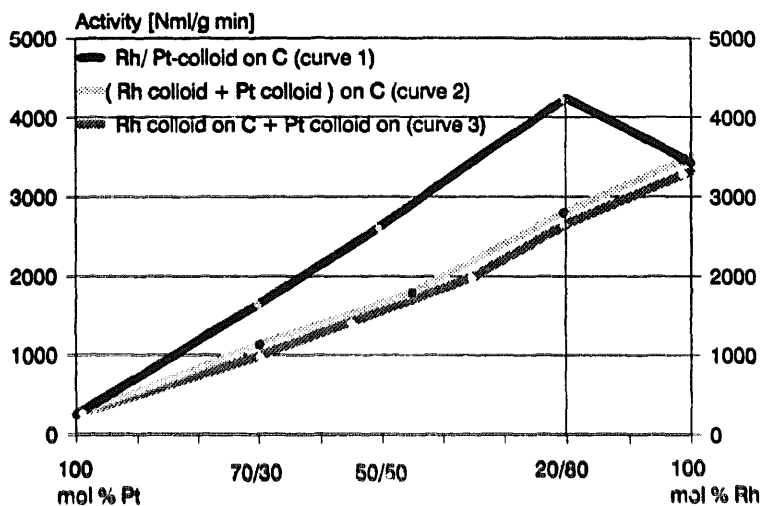


Fig. 12. Comparison of the activity of alloyed and mixed Rh-Pt-C catalysts in the crotonic acid test.

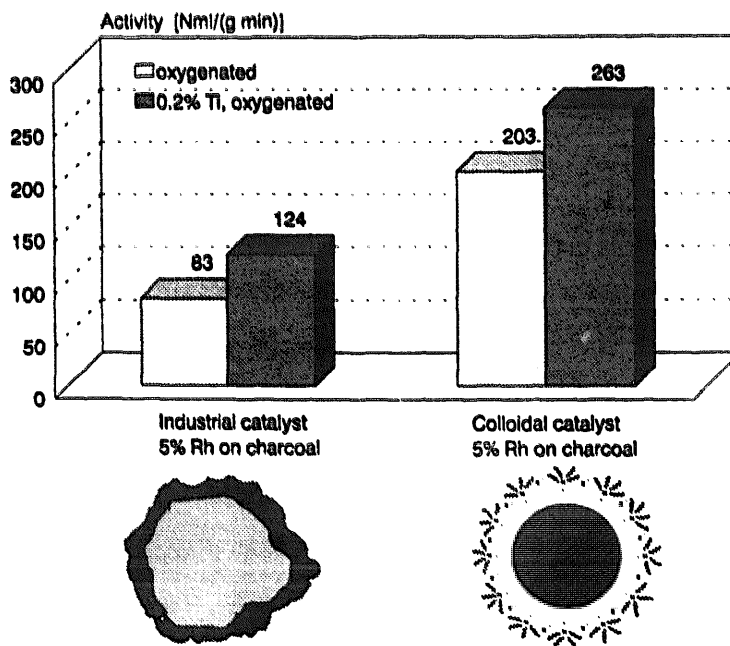
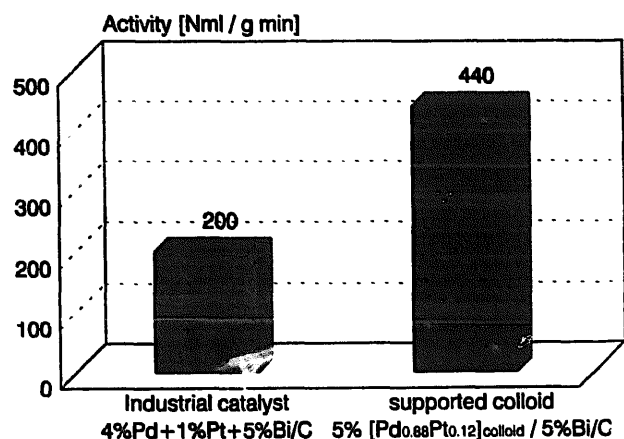


Fig. 13. Catalytic hydrogenation of butyronitrile on Rh colloid catalysts.



conditions:  
 $O_2$ -pressure = 1 bar  
 $T = 30^\circ C$   
 $[glucose] = 0,88 M$   
 $\frac{[glucose]}{[noble\ metal]} = 2065$

Fig. 14. Initial activity in the catalytic oxidation of D-glucose on bismuth-promoted Pd–Pt–C colloid catalysts.

In contrast, the corresponding activity plot of the bimetallic Pt–Rh colloid systems [90,91] clearly shows a maximum at Pt<sub>20</sub>Rh<sub>80</sub>. Since this maximum exceeds the activity found for Rh colloid–C alone, this finding indicates a synergistic effect.

The superior properties of the new type of bimetallic colloid catalyst formed by the adsorptive fixation of surfactant-stabilized bimetallic precursor particles to the support, compared with conventional 'bimetallic' catalysts prepared via co-impregnation of two metal salts followed by calcination, were confirmed in the catalytic oxidation of e.g. D-glucose by molecular oxygen giving D-gluconic acid using a bismuth-promoted Pd–Pt colloid as the active component on a charcoal support (see Fig. 14) [107].

The carbohydrate oxidation reaction shown in Fig. 14 is currently under intensive investigation both in academia [108] and industry [109,110]. In our study we first compared the activity of a conventionally prepared catalyst from industry (atomic ratio Pd:Pt = 4:1, supported on charcoal) with the activity of a Pd<sub>88</sub>–Pt<sub>12</sub> colloid supported on an identical sample of charcoal. Both catalysts were promoted by bismuth. The results are shown in Fig. 14. Without affecting the high selectivity of the reaction (98%), the catalytic activity of the supported bimetallic Pd–Pt colloid was found to be virtually doubled.

The improved activity of the Pd–Pt colloid catalyst may be explained — in addition to the true bimetallic composition of the active component — by the fact that the adsorbed precursor particles sit at the most exposed sites of the support; consequently, they are more accessible for the substrates than the conventional type of catalyst made via salt impregnation, where part of the metal is inevitably 'buried' under the support surface. The practical disadvantage of highly active catalyst components sitting on exposed positions of the support often lies in a rather insufficient long term stability because the sensitivity to poisons is drastically increased. Fig. 15 compares the stability of an optimized conventional catalyst with the colloidal Pd–Pt system. Surprisingly, the expected decay in activity after recycling the catalysts was found to be much less in the case of the colloidal than in the conventional system [107].

Since chemisorption measurements indicate that metal colloid precursors adsorbed on the surface of the support are still partly covered by surfactant molecules [111], it seems reasonable to assume that the catalytically active nanometal particles are protected by a 'coat' which, although permeable to small molecules such as H<sub>2</sub> or O<sub>2</sub>, prevents the direct contact with poisons.

In order to check the possible influence of stabilizing groups on the catalytic properties of colloidal nanomet-

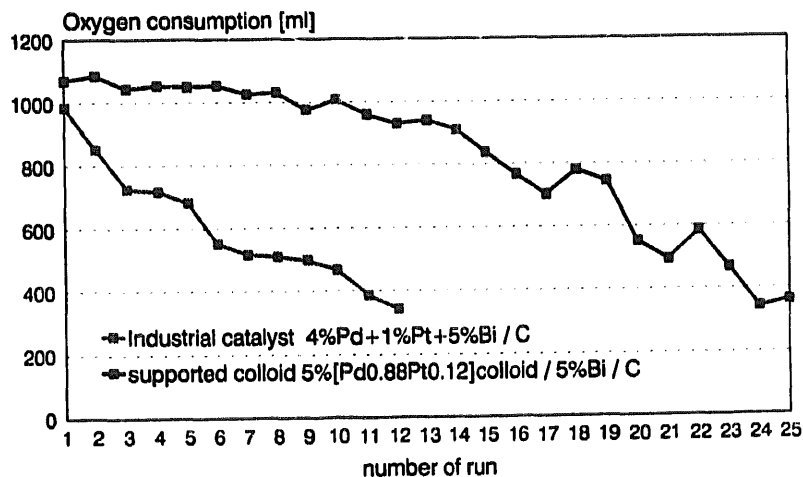
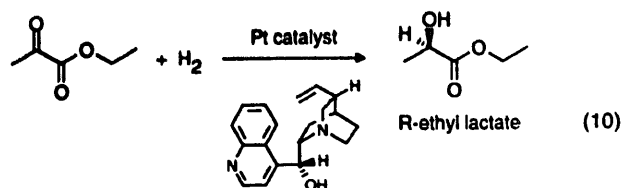


Fig. 15. Conversion decay after recycling of the Pd–Pt–C oxidation catalysts (reaction time 40 min).



als we have investigated the stereoselectivity of colloidal platinum (particle size 2 nm) stabilized by a chiral ammonium group derived from dihydrocinchonidine in the enantioselective hydrogenation of ethyl pyruvate (Eq. 10) [112].

The enantioselectivity control of conventional heterogeneous Pt catalysts in the reaction (Eq. 10) using modifiers derived from cinchona alkaloids is well established in the literature, and ee values above 90% have been reported [113–115]. Further, the influence of con-

version and bulk diffusion limitations on the stereoselectivity was recently studied in detail [116].

Unsupported colloidal Pt of 2.0 nm particle size stabilized by dihydrocinchonidonium acetate gave, in homogeneous acetic acid solution under the conditions quoted in Section 7.4.2, the R-ethyl lactate in 70% ee. This clearly suggests a strong selectivity control of the catalytic reaction induced by the chiral ammonium group present at the surface of the colloid particle. Our current investigations have further revealed that the alkaloid derivative acts as an 'accelerating ligand' in favor of the formation of the R enantiomer. Consequently, the ee values increase when higher concentrations of H<sub>2</sub> are applied in solution. In homogeneous phase, however, the Pt colloid tends to precipitate when pressurized hydrogen is applied. Therefore, we have adsorbed the Pt colloid to SiO<sub>2</sub> and Al<sub>2</sub>O<sub>3</sub> supports. The resulting chiral modified heterogeneous Pt colloid catalysts performed the reaction (Eq. 10) under 10 MPa of hydrogen

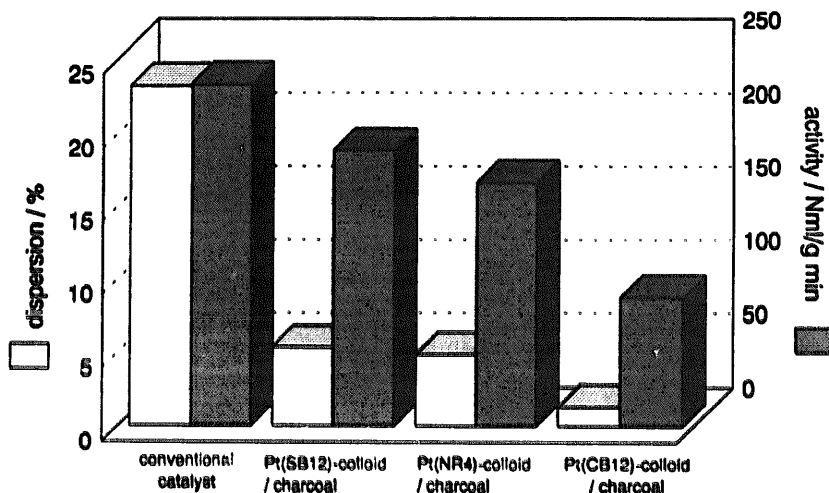


Fig. 16. Metal dispersion (surface accessibility) and hydrogenation activity (crotonic acid test) of Pt colloid catalyst protected by different surfactants compared with a conventional Pt catalyst.

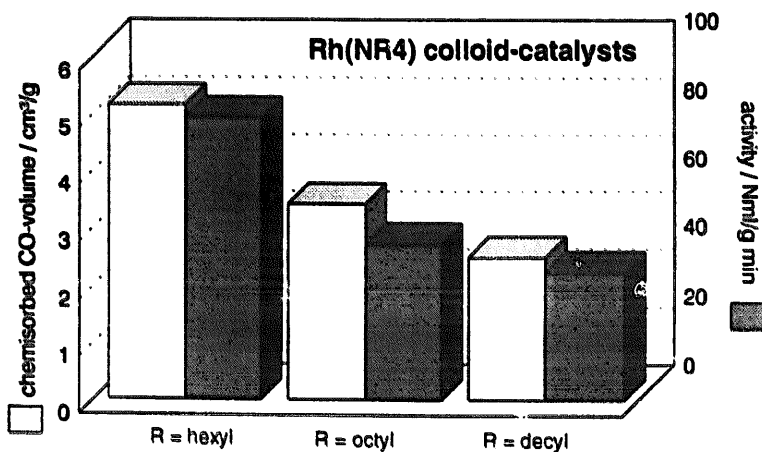


Fig. 17. Influence of the alkyl chain length in N(R)<sub>4</sub>-stabilized Rh colloid catalysts on CO chemisorption and hydrogenation activities (butyronitrile test).

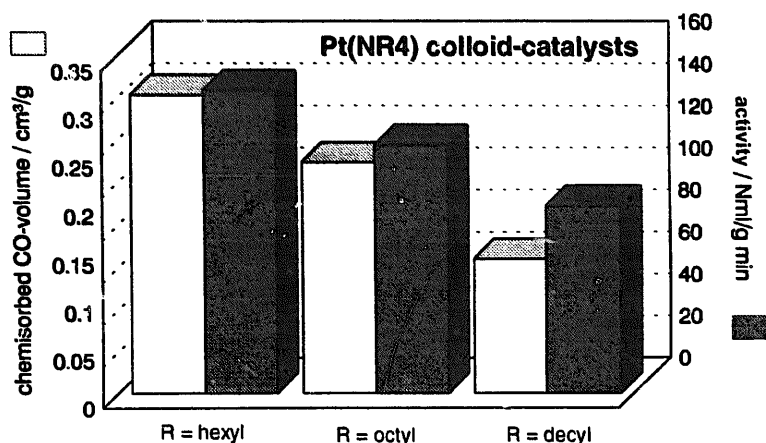


Fig. 18. Influence of the alkyl chain length in  $N(R)_4^+$ -stabilized Pt colloid catalysts on CO chemisorption and hydrogenation activities (crotonic acid test).

giving the *R* enantiomer in 81% and 85% ee respectively.

## 6. Influence of the protecting shell

### 6.1. Accessibility by CO chemisorption

The CO chemisorption of several 5 wt.% Pt colloid–charcoal catalysts was investigated by the static method and correlated to their hydrogenation activity in the crotonic acid test [83]. The mean particle size of the colloids is 2.3 nm. The results were compared with the conventional 5 wt.% Pt–charcoal catalyst F 103 R/D (Degussa AG) (see Fig. 16). The accessible metal surface of the colloid catalysts was found to be much smaller (dispersion between 1 and 5%) than the metal surface of the conventional catalyst (dispersion 24%). Variation of the protecting agent alters the accessibility of the metal surface and consequently the hydrogenation

activity (87, 150, 190 N ml g<sup>-1</sup> min<sup>-1</sup>). The most active colloid catalyst reaches nearly the same activity as the industrial catalyst (232 N ml g<sup>-1</sup> min<sup>-1</sup>). However, the catalytic activity is not strictly governed by the surface accessibility. In the case of colloid catalysts the protecting shell covers the metal surface, but the hydrogenation activity of those catalysts is still high enough because hydrogen penetrates through the protecting shell. Consequently, metal colloid catalysts often show an improved lifetime, because the protecting shell prevents the metal surface from being poisoned (compare Figs. 11 and 15).

The accessibility of the metal surface may even be controlled by the steric demand of the protecting shell. The accessibility of the metal surface and the hydrogenation activity using the crotonic acid test (Pt) or the butyronitrile test (Rh) [83] depends on the alkyl chain length of the  $NR_4^+$  protecting shell for Pt (Fig. 17) and Rh (Fig. 18) colloid catalysts (R = hexyl, octyl or decyl) [85,87]. The hydrogenation activity of the Rh– $NR_4^+$

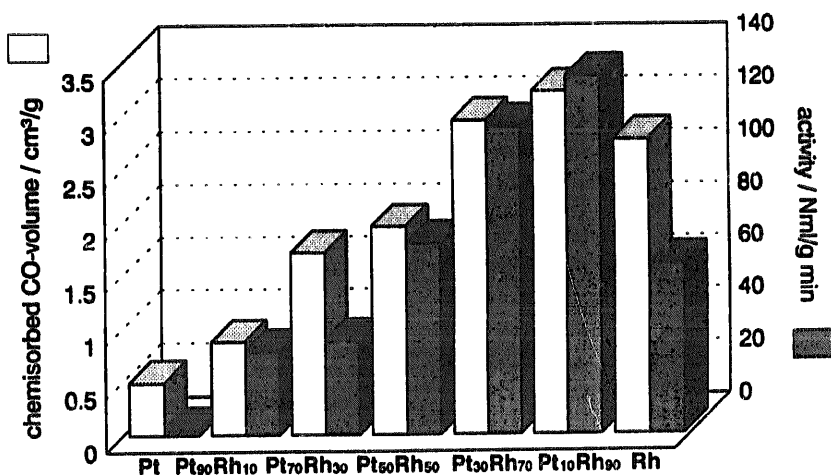


Fig. 19. Synergistic effect of colloidal Pt<sub>n</sub>Rh<sub>m</sub> alloy catalysts monitored by CO chemisorption.

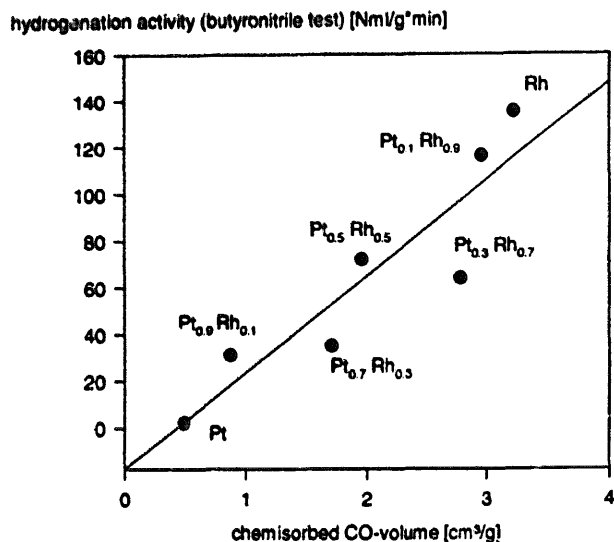


Fig. 20. Correlation of the hydrogenation activity with the CO chemisorption values of Pt<sub>n</sub>Rh<sub>m</sub> alloy catalysts.

colloid catalyst varies between 37 and 82 N ml g<sup>-1</sup> min<sup>-1</sup>, when R is changed from decyl to hexyl and in the same order the CO uptake varies between 2.48 and 5.14 cm<sup>3</sup> g<sup>-1</sup>. In the case of Pt-NR<sub>4</sub><sup>+</sup> colloid catalysts the CO uptake varies between 0.14 (R = decyl) and 0.31 cm<sup>3</sup> g<sup>-1</sup> (R = hexyl). However, the differences in CO chemisorption are much smaller in the case of Pt catalysts than in the case of Rh catalysts. The hydrogenation activities of the Pt catalysts vary between 89 (R = decyl) and 144 N ml g<sup>-1</sup> min<sup>-1</sup> (R = hexyl). With increasing chain length of the alkyl group R the accessible metal surface measured by CO chemisorption and the hydrogenation activity decreases. The CO up-

take correlates with the activity both in the case of Rh and Pt catalysts.

### 6.2. Bimetallic effects in catalysis monitored by CO chemisorption

In order to monitor the synergic effect of Pt and Rh found in colloidal Pt-Rh bimetallic catalysts (see Fig. 12), both the CO chemisorption and the hydrogenation activity (butyronitrile test) of a series of Pt<sub>n</sub>-Rh<sub>m</sub>-N(octyl)<sub>4</sub><sup>+</sup> colloid catalysts [83] were compared. The CO uptake varies between 0.49 cm<sup>3</sup> g<sup>-1</sup> for the pure Pt catalyst and 2.78 cm<sup>3</sup> g<sup>-1</sup> for the pure Rh catalyst. For the Pt<sub>10</sub>Rh<sub>90</sub> alloy catalyst a maximum value of 3.23 cm<sup>3</sup> g<sup>-1</sup> was found, which corresponds with the catalytic activities of the various alloy compositions (butyronitrile test). Figs. 19 and 20 show the good correlation between CO chemisorption and hydrogenation activity.

### 6.3. IR investigation of chemisorbed CO species

Supplementary to the CO chemisorption studies on supported colloids we have investigated chemisorbed CO species by IR spectroscopy on free-metal colloids [6,117,118] and on different supports. Fig. 21 shows the IR spectra of CO adsorbed on a free N(octyl)<sub>4</sub><sup>+</sup>-stabilized Rh colloid (a), a free sulfobetaine-stabilized Rh colloid (b) and a sulfobetaine-stabilized Rh colloid supported on alumina (c).

The spectra of the free colloids ((a) and (b)) show four main IR absorptions which can be assigned to three different Rh-CO species: geminal Rh(CO)<sub>2</sub> (2064 + 1988 cm<sup>-1</sup>), terminal Rh-CO (2000 cm<sup>-1</sup>(sh)) and

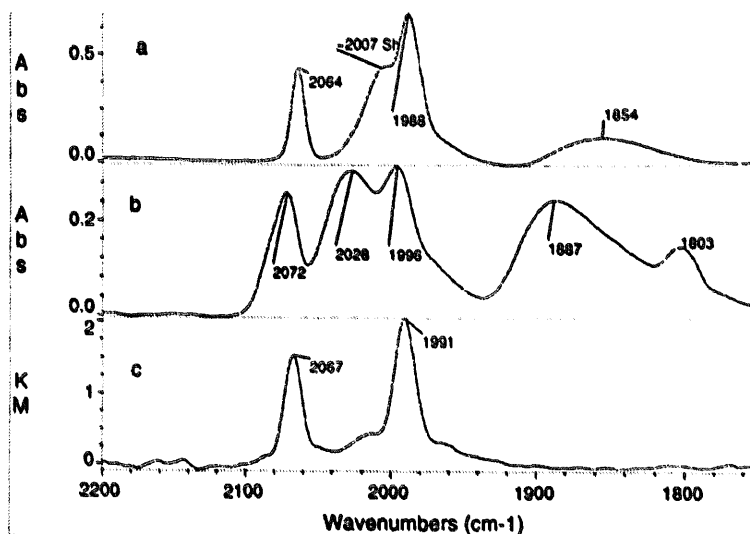


Fig. 21. IR spectra of adsorbed CO on an N(octyl)<sub>4</sub><sup>+</sup>-stabilized Rh colloid (a), sulfobetaine-12-stabilized Rh colloid (b), sulfobetaine-12-stabilized Rh colloid supported on alumina (c).

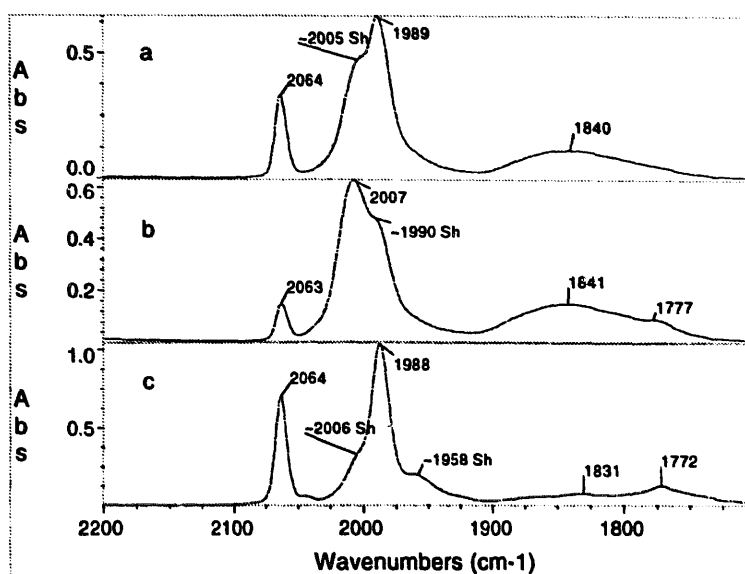


Fig. 22. IR spectra of adsorbed CO on an  $N(\text{octyl})_4^+$ -stabilized Rh colloids in different oxidation states without pretreatment (a), hydrogen pretreated (b), after oxidation by air (c).

bridged  $\text{Rh}_2\text{CO}$  ( $1854\text{ cm}^{-1}$ ). For the sulfobetaine-stabilized Rh colloid, these IR absorptions are shifted slightly to higher wavenumbers, which may be an effect of particle size. The geminal  $\text{Rh}(\text{CO})_2$  represents an oxidized  $\text{Rh}^{1+}$  species, whereas the frequencies for the terminal and bridged CO are typical for  $\text{Rh}^0$ . The supported Rh colloid exhibits only two IR absorptions corresponding to geminal  $\text{Rh}(\text{CO})_2$  at  $2067$  and  $1991\text{ cm}^{-1}$ . This pattern has been found with supported Rh colloids on alumina, titania, silica and charcoal. In the literature a mechanism is proposed [119–121] where  $\text{Rh}^0$  is oxidized to  $\text{Rh}^{1+}$  in the presence of CO by the hydroxyl groups on the support, forming a species of the type support-O- $\text{Rh}^{1+}(\text{CO})_2$ .

The influence of the oxidation state of Rh surface atoms on the adsorbed CO species is shown in Fig. 22. First, CO was adsorbed on sample (a) without any pretreatment. Colloid sample (b) was pretreated with hydrogen, a second sample (c) was air oxidized before CO adsorption. Sample (a) exhibits four IR absorption bands at  $2064/1989$ ,  $2005(\text{sh})$  and  $1840\text{ cm}^{-1}$  (a). CO adsorbed on sample (b) shows an increased intensity for the absorptions at  $2007$  and  $1841\text{ cm}^{-1}$  compared with the colloid (a). The IR absorption bands at  $2064$  and  $1989\text{ cm}^{-1}$  of the  $\text{Rh}(\text{CO})_2$  species are decreased. Obviously, a part of the oxidized  $\text{Rh}^{1+}$  species was reduced by hydrogen. In contrast, the air pretreated colloid (c) shows increased absorptions at  $2064$  and  $1988\text{ cm}^{-1}$ , while the absorptions at  $2006$  and  $1830\text{ cm}^{-1}$  almost disappeared, indicating that nearly the whole Rh surface was oxidized. The IR spectra show that the hydrogen pretreatment causes a decrease of the  $\text{Rh}(\text{CO})_2$  species while the air treatment causes an

increase of  $\text{Rh}(\text{CO})_2$  species. Using IR evidence, the intensity of the  $\text{Rh}(\text{CO})_2$  absorptions indicates the oxidation state of the Rh atoms on the particle surface.

Work is currently in progress to explore further the scope and limitations of nanosized metal colloids as precursors for a new type of highly active, stable, and selective catalyst.

## 7. Experimental

All reductions using metals or hydrides were carried out under argon in dry organic solvents. Using hydrogen for reductions in aqueous solution, deoxygenated water was used.

### 7.1. Organosols

#### 7.1.1. THF-stabilized Ti, Zr, V, Nb, and Mn organosols

70 ml of a 1.15 M solution of  $\text{K}[\text{BEt}_3\text{H}]$  (80 mmol) in THF were added at room temperature over 2 h to a stirred suspension of  $\text{TiBr}_4 \cdot 2\text{THF}$  (10.24 g, 20 mmol) in THF. During the reaction approximately 20 mmol of  $\text{H}_2$  were released. The reaction mixture was stirred for another 2 h at room temperature. The precipitated  $\text{KBr}$  was removed by filtration.  $\text{BEt}_3$  and THF were removed from the brown filtrate in vacuo. The product was dried in vacuo for 16 h. Yield: 1.61 g (79%), 9.3 g (99%)  $\text{KBr}$ . IR:  $\nu(\text{cm}^{-1})$  867s, 915vw, 1035s, 1340br, 1455w;  $^1\text{H NMR}$  ( $[\text{D}_8]\text{THF}$ , 300 K, TMS):  $\delta$  1.77 (m, 2H), 3.61 (m, 2H); MS:  $M/z$  72 ( $\text{C}_4\text{H}_8\text{O}^+$ ); protonolysis with 2 N HCl yielded 1.5 mol  $\text{H}_2/\text{Ti}$ .

The organosols of Zr, V, Nb and Mn were prepared in an analogous manner.

Starting materials:  $\text{ZrBr}_4 \cdot 2\text{THF}$ ;  $\text{VBr}_3 \cdot 3\text{THF}$ ;  $\text{NbCl}_3 \cdot 2\text{THF}$ ;  $\text{MnBr}_2 \cdot 2\text{THF}$ .

#### 7.1.2. Tetrahydrothiophene-stabilized Ti and V organosols

45.1 mmol of  $\text{K}[\text{BEt}_3\text{H}]$  dissolved in 40 ml of tetrahydrothiophene were added at room temperature over 3 h to 2.13 g of  $\text{TiCl}_4$  (11.3 mmol) in 50 ml of tetrahydrothiophene. Hydrogen was developed and a precipitation of KCl was formed. The resulting black reaction mixture was filtered and all volatile compounds were removed in vacuo. The product was dried in vacuo for 16 h. Elemental analysis: C, 8.87%; H, 1.55%; B, 0.18%; Cl, 35.22%; K, 15.70%; S, 8.33%; Ti, 12.40%. IR:  $\nu(\text{cm}^{-1})$  880vw, 1260s, 1440w, 2860w, 2940w.

The organosol of V was prepared in an analogous manner using  $\text{VBr}_3$ .

#### 7.1.3. $\text{NR}_4\text{Cl}$ -protected Ir organosol

A solution of  $\text{N}(\text{C}_8\text{H}_{17})_4[\text{BEt}_3\text{H}]$  in THF (50 ml, 0.37 M) was added within 1 h at room temperature to a stirred suspension of anhydrous  $\text{IrCl}_3$  (1.84 g, 6.1 mmol) in 200 ml of THF. Almost complete dissolution of the  $\text{IrCl}_3$  occurred after 16 h at 60 °C. After filtration the clear, dark black-brown solution was concentrated in vacuo, and the black-brown, waxy residue was dried for 3 h at room temperature and 0.1 Pa. The product (7.38 g) was soluble in THF, ether, toluene and acetone, but insoluble in ethanol, and contained 10.85% Ir. The residue was suspended in 200 ml technical quality ethanol without protective gas and addition of 20 ml technical quality ether caused a grey-black precipitate to form. This was left to stand for 1 h, before removing the clear supernatant solution by inert gas pressure (argon) on the liquid surface. The precipitate was washed once with a mixture of 40 + 4 ml ethanol + ether. Drying in vacuum (0.1 Pa, 1 h, room temperature) yielded a grey Ir colloid powder (0.36 g), which was very soluble in THF, soluble in acetone and insoluble in ether, ethanol and toluene. Elemental analysis: C, 19.97%; H, 3.49% Ir, 65.55%; N, 0.27%. Mean particle size (TEM): 1.5 nm.

#### 7.1.4. $\text{NR}_4\text{Br}$ -protected Pd organosol

0.5 g (2.23 mmol)  $\text{Pd}(\text{CH}_3\text{CO}_2)_2$  and 1 g (1.30 mmol)  $\text{N}(\text{dodecyl})_4\text{Br}$  were dissolved in 110 ml of THF. The flask was evacuated several times and then  $\text{H}_2$  was introduced via a gas burette under normal pressure. After a while the solution turned black and after 16 h 60.4 N ml (120%) of  $\text{H}_2$  had been taken up. THF was added to give a total volume of 110 ml and on addition of 55 ml of  $\text{H}_2\text{O}-\text{Ar}$ , a brown-black precipitate resulted. After standing for 16 h the supernatant liquid was siphoned off and the solid was dried for 3 h in

vacuum (0.1 Pa). The black powder isolated in this manner was redispersible in THF. Yield: 0.27 g (87%). Elemental analysis: C, 13.19%; H, 2.47%; Br, 3.06%; N, 1.64%; Pd, 76.73%. XPS: Pd(0). Mean particle size (TEM): 1.8 nm.

#### 7.1.5. $\text{NR}_4^+$ -protected Cr, Mo, Cu, Ag, and Au organosols

20 ml of a 0.29 M solution of  $\text{N}(\text{octyl})_4[\text{BEt}_3\text{H}]$  (5.8 mmol) in toluene were added at room temperature to a vigorously stirred suspension of  $\text{CrCl}_3$  (0.311 g, 1.96 mmol) in 200 ml of toluene. Thereafter the reaction mixture was ultrasonically treated for 2 h and all volatile compounds of the resulting black solution were evaporated in vacuo (0.1 Pa). Drying in vacuum (0.1 Pa, 16 h, room temperature) yielded a black viscous chromium colloid, which proved to be very soluble in toluene and THF, and insoluble in ether and pentane. (The solutions of the colloid are air-sensitive.) Mean particle size (TEM): 1.5 nm.

The organosols from Mo, Cu, Ag, and Au were prepared in an analogous manner using  $\text{MoCl}_3$ ,  $\text{CuCl}_2$ , Ag neodecanoate, and  $\text{AuBr}_3$  as starting materials. Mean particle sizes (TEM): Mo, 2–3 nm; Cu, 8.3 nm; Ag, 15 nm; Au, 10 nm.

#### 7.1.6. $\text{NR}_4\text{Br}$ -protected Fe organosol

A solution of 23.8 mmol of  $\text{N}(\text{C}_8\text{H}_{17})_4[\text{BEt}_3\text{H}]$  in THF (70 ml, 0.34 M) was added within 3 h at 60 °C to a stirred suspension of anhydrous  $\text{FeBr}_2$  (2.47 g, 11.45 mmol) in 400 ml of THF. The color changed from brown-orange to deep black-red and after 16 h at 60 °C precipitated magnetic iron was filtered off at 20 °C. The clear solution was concentrated in vacuo at room temperature, and the black, viscous residue was dried for 16 h at room temperature and 0.1 Pa. The air-sensitive magnetic product (7.23 g) was soluble in THF, toluene and acetone, but insoluble in ether, ethanol, and pentane and contained 4.5% Fe. Mean particles size (TEM): 3.0 nm. The residue was dissolved in 50 ml of THF and addition of 120 ml pentane caused a grey-black precipitate to form. This was left to stand for 1 h before removing the clear supernatant solution on the liquid surface. Drying in vacuum (0.1 Pa, 16 h, room temperature) yielded a grey iron colloid powder (1.97 g), which was soluble in THF and toluene. Metal content: 14.34% Fe. Mean particle size (TEM): 3.0 nm.

#### 7.1.7. Oxygenation of the Fe organosol to Fe oxide organosol

0.5 g iron colloid (4.5% Fe) was dissolved in 50 ml of THF under argon atmosphere and the resulting clear black-red solution was slowly stirred for 16 h after opening of the flask. The color of the solution changed to rusty-brown without any precipitation of agglomerated iron. This solution can be handled for a longer time



in air, but evaporation of the solution resulted in an insoluble powder.

#### 7.1.8. Rh colloid via $H_2$ reduction in the presence of trialkylamines

2.0 g (7.6 mmol) of  $RhCl_3 \cdot 3H_2O$  and 16.13 g (45.6 mmol) of  $N(C_8H_{17})_3$  were dissolved without protecting gas in 200 ml of THF. The intense red solution was introduced into a 500 ml autoclave and hydrogen was added to a pressure of 5 MPa. After stirring for 16 h at 60 °C, the hydrogen was released, and a clear, deep brown-black solution discharged. The volatile compounds were removed through evaporation. Drying under vacuum (0.1 Pa, 4 h, 40 °C) resulted in a waxy black residue which proved to be very soluble in THF, toluene, and acetone and partly soluble in ether and ethanol. Thereafter, the residue was dissolved in 300 ml of technical quality ether without using an inert gas atmosphere which caused the formation of a dark grey precipitate. The precipitate was allowed to settle for ca. 1 h before the clear supernatant solution was removed by applying pressure of an inert gas on the liquid surface. Drying under vacuum (0.1 Pa, 5–10 min, 20 °C) yielded a greyish-black colloidal powder (0.68 g) which proved to be very soluble in THF and insoluble in ether, acetone, toluene and ethanol. Elemental analysis: C, 27.38; H, 4.86; Cl, 4.61; N, 1.76; Rh, 60.99 wt%. Mean particle size (TEM): 2.4 nm. Mass spectrum  $m/z$ : 353 [ $(C_8H_{17})_3N$ ],  $M^+$ , 254 [ $(C_8H_{17})_2NCH_2$ ], 36 (HCl). IR (KBr): ( $cm^{-1}$ ) 2920, 2855, 2450 ( $N^+H$ ), 1465, 1380, 722.

## 7.2. Hydrosols

#### 7.2.1. SB12-protected Pt colloid in water

1.4 g (5.3 mmol)  $PtCl_2$ , 7.2 g (21.2 mmol) SB12 and 0.4 g (5.3 mmol)  $Li_2CO_3$  were stirred in 10 ml of  $H_2O$  and  $H_2$  was introduced under normal pressure for 3 h at 20 °C. After ca. 30 min a clear black solution formed and all volatile compounds were evaporated in vacuum (0.1 Pa, 40 °C). The resulting black powder was redispersible in water. Yield: 8.4 g. Metal content: Pt 10.7%. Mean particle size (TEM): 2.2 nm.

#### 7.2.2. Polyoxyethylenelaurylether-protected Pt–Pd colloid in water

1.35 g (2.65 mmol)  $H_2PtCl_6 \cdot 6H_2O$  and 0.7 g (2.65 mmol)  $Pd(NO_3)_2 \cdot H_2O$  were dissolved together with 7 g polyoxyethylenelaurylether and 1.0 g (13.25 mmol)  $Li_2CO_3$  under argon in 100 ml  $H_2O$ , and for 4 h  $H_2$  gas was passed through it at 20 °C. The resultant deep black reaction mixture was filtered over a D4 glass frit, and the deep black clear solution was concentrated in high vacuum (0.1 Pa, 40 °C) to dryness. 11.2 g Pt–Pd colloid

was obtained in the form of a black solid having a metal content of 4.3% Pt and 2.3% Pd.

#### 7.2.3. Water-soluble Pt colloid stabilized by dihydrocinchonidine

0.104 g  $PtCl_4$  (0.31 mmol) were dissolved in a 100 ml two-neck flask, provided with reflux condenser and a septum, in 80 ml distilled water, and heated to reflux temperature in an oil bath. The temperature of the oil bath was  $140 \pm 5$  °C during the synthesis. A solution of 0.092 g dihydrocinchonidine (0.31 mmol) in 7 ml of 0.1 N formic acid was rapidly injected through the septum. In the beginning, the reaction mixture became turbid and began to turn black after some minutes. The reaction was finished approximately 10 min after the start of the black coloration. (If the formed platinum colloids are to be applied on carrier materials, the aqueous product dispersion can be used without isolation of the metal particles before the fixing on the carrier.) The reaction mixture was frozen in liquid nitrogen, and water and hydrochloric acid removed by freeze drying. A black powder is obtained which can be completely dispersed in water. The yield is 0.18 g (103% of the theory). Elemental analysis: C, 39.5%; H, 5%; Cl, 16%; N, 5%; Pt, 24.5%. TEM examinations show an average particle size of 2 nm.

#### 7.2.4. Polyoxyethylenelaurylether-protected Pt–Rh colloid in water

1.35 g (2.65 mmol)  $H_2PtCl_6 \cdot 6H_2O$  and 0.7 g (2.65 mmol)  $RhCl_3 \cdot H_2O$  were dissolved together with 7 g polyoxyethylenelaurylether and 1.0 g (13.25 mmol)  $Li_2CO_3$  under argon in 100 ml  $H_2O$ , and over 20 h a solution of 2.86 g (55.0 mmol) Li formate in 50 ml  $H_2O$  was added at 60 °C. The resultant deep black reaction mixture was filtered over a D4 glass frit, and the deep black clear solution was concentrated in high vacuum (0.1 Pa, 40 °C) to dryness. 12.5 g Pt–Rh colloid were obtained in the form of a black solid having a metal content of 4.0% Pt and 2.0% Rh.

## 7.3. Preparation of the catalysts

#### 7.3.1. Preparation of a Pd (SB12)-activated carbon catalyst for the partial oxidation of carbohydrates (5 wt.% Pd on C)

1.254 g of a microporous powdery active carbon having a grain size of 20  $\mu m$  were suspended in 50 ml deoxygenated  $H_2O$ , and 64.7 ml of a solution of Pd (SB12) colloid in deoxygenated water (1.02 mg Pd  $ml^{-1}$ ) added within 16 h under stirring. The treated carbon is separated over a glass frit yielding a colorless filtrate. This was washed twice with 25 ml deoxygenated water and dried over 16 h in vacuum (0.1 Pa) at room temperature. Subsequently, the catalyst was oxy-

generated over 16 h at 10 Pa (approximately 0.2% O<sub>2</sub>). The resulting catalyst can be handled at air.

### 7.3.2. Preparation of a heterogeneous Pt catalyst by adsorption of Pt–dihydrocinchonidine colloid on SiO<sub>2</sub> and activated carbon

100 ml of the colloid solution, described in Section 7.2.3., were directly taken up after the synthesis in 100 ml cold, distilled water, and added dropwise over 1 h into 100 ml of the carrier suspension in water. Either the highly disperse silicon dioxide Aerosil P 25™ (Degussa) or the active carbon carrier 196 (Degussa) (which was oxidized with NaOCl before the fixing of the colloid to the carrier) can be used as carriers. The resulting suspensions were stirred with a magnetic stirrer at a low rotational speed for 2 days and then filtered. The filtrate is completely decolorized, from which it can be concluded that the metal colloids were quantitatively absorbed on the carrier. The resulting heterogeneous Pt catalysts were dried in a drying oven, and could be used subsequently as hydrogenation catalysts without further intermediary steps. A uniform and agglomeration-free distribution of the colloids on the carrier materials was shown by TEM examination.

## 7.4. Catalysis

### 7.4.1. Use of the Pd (SB12)–activated carbon catalyst for the oxidation of glucose to gluconic acid

100 ml of an aqueous solution of glucose with 16 g (88 mmol) glucose (99 wt.%) and 0.24 g of the catalyst described in Section 7.3.1. (1.5 wt.% in relation to the amount of glucose) were transferred to a 250 ml stirring reactor equipped with gassing stirrer, thermometer, alkali metering, pH electrode and oxygen inlet. The oxygen is distributed at normal pressure by means of the gassing stirrer in the solution at a reaction temperature of 56 °C. The resulting gluconic acid is neutralized by addition of aqueous 10 wt.% sodium hydroxide. The final pH value of the suspension was 10.0. The catalyst was filtered off, and the filtrate analyzed by means of ion chromatography and HPLC.

### 7.4.2. Enantioselective hydrogenation of ethyl pyruvate to ethyl lactate

A 100 ml autoclave was charged with 100 mg of the catalyst, described in Section 7.3.2 (Pt on SiO<sub>2</sub>; metal content 5%), 5 ml (45 mmol) ethyl pyruvate, 20 mg (0.1 mmol) dihydrocinchonidine, 10 ml acetic acid and a 3 cm magnetic stirring bar. The pressure vessel was degassed after closure and, subsequently, 10 MPa hydrogen was introduced under vigorous stirring. The reac-

tion took place at 25 °C, and lasted approximately 15 min. Following the venting of the pressure vessel, the product mixture was separated from the catalyst by filtration, the clear filtrate neutralized with sodium bicarbonate solution and subsequently extracted with diethyl ether. After removing the solvent, 3.5 g of a clear liquid was obtained, corresponding to 70% isolated yield. This was identified as ethyl lactate by NMR and mass spectroscopy. The conversion was determined by gas chromatography to be 100%. The optical yield of the reaction was examined by gas chromatography on a chiral column, and yields an excess of enantiomer of 81%.

## 7.5. Chemisorption measurements

### 7.5.1. CO chemisorption

Chemisorption measurements on colloid/support catalysts were carried out with a Micromeritics ASAP 2000 Chemi system instrument. The samples were degassed at 150 °C and 10<sup>-4</sup> Pa for 16 h, reduced with hydrogen at 40 °C for 1 h and evacuated at 90 °C for 2 h. After this pretreatment the CO chemisorption isotherm was measured and after 30 min evacuation the CO physisorption was measured. The physisorbed CO volume was subtracted from the adsorbed CO volume of the first isotherm and from the difference the accessible metal surface area was calculated.

### 7.5.2. CO adsorption on colloids in solution

100 mg colloid was dissolved under argon in ca. 50 ml of THF (N(octyl)<sub>4</sub><sup>+</sup>-stabilized colloid) or water (SB12-stabilized colloid). CO was bubbled through these solution for 30 min. The solvent was then evaporated in vacuo (0.1 Pa). The IR spectra were recorded with a Nicolet FTIR spectrometer 7199 as KBr pellets or (in the case of waxy substances) between two KBr plates. The supported colloids were measured in the diffuse reflectance mode.

## Acknowledgements

The authors gratefully acknowledge the valuable support of the following scientists, companies and institutions: Dr. B. Tesche, Fritz-Haber-Institut der MPG, Berlin (now at MPI für Kohlenforschung, Mülheim), for numerous TEM images taken with a Siemens Elmiskop 102 and DEEKO 100 at 100 kV and many helpful discussions; Mr. T. Kamino, Hitachi Instruments Engineering Co. Ltd., 882 Ichige, Katsuta-shi (Japan), and Dipl. Ing. B. Spliethoff, MPI für Kohlenforschung, Mülheim, for HRTEM images performed with a Hitachi HF 2000 at 200 kV including EDX point analyses. Professor Dr. R. Courths and Dipl.-Phys. B. Heise,

Universität-Gesamthochschule Duisburg, for XPS spectra obtained using an Escalab Mark II. Professor Dr. W. Keune and Dipl.-Ing. U. von Hörsten, Universität-Gesamthochschule Duisburg, for the measurement and interpretation of the Mössbauer spectra. Professor Dr. J. Rozière, Dr. D.J. Jones, Université Montpellier (France), for the X-ray absorption measurements recorded on the Ti K-edge (77 K) with an EXAFS 3 spectrometer in DCI (French Synchrotron Facility in Lure). Professor Dr. J. Hormes, Dr. R. Franke, Dipl.-Phys. Rothe and Dipl.-Phys. Becker, Universität Bonn, for XPS, XANES, and EXAFS measurements on the Pt–Rh–colloid samples using synchrotron radiation at beamline BN3 of the storage ring ELSA at Bonn university. Further, we are indebted to Professor Dr. P. Kleinschmit and Dr. P. Panster and Dr. A. Freund, Degussa AG, ZN Wolfgang, Hanau, for a gift of commercial noble metal catalysts and the test procedures for noble metal charcoal catalysts. The support of this work by Fonds der Chemischen Industrie, Frankfurt and a grant from the German Ministry of Education, Science, Research, and Technology (BMBF FKZ 03 D 0007 A2) is also gratefully acknowledged.

## References

- [1] G. Schmid (ed.), *Clusters and Colloids*, VCH, Weinheim, 1994.
- [2] M. Boutonnet, J. Kizling, P. Stenius and G. Maire, *Colloids Surf.*, **5** (1982) 209.
- [3] M. Boutonnet, J. Kizling, R. Touroude, G. Maire and P. Stenius, *Appl. Catal.*, **20** (1986) 163.
- [4] J.S. Bradley, *Adv. Organomet.*, **6** (1983) 687.
- [5] J.S. Bradley, E. Hill, M.E. Leonowicz and H.J. Witzke, *J. Mol. Catal.*, **41** (1987) 59.
- [6] J.S. Bradley, J.M. Millar, E.W. Hill, S. Behal, B. Chaudret and A. Duteil, *Faraday Discuss.*, **92** (1991) 225.
- [7] P. Braunstein, *Nouv. J. Chim.*, **10** (7) (1986) 365.
- [8] K. Esumi, M. Shiratori, H. Ishizuka, T. Tano, K. Torigoe and K. Meguro, *Langmuir* **7** (1991) 457.
- [9] K. Meguro, M. Torizuka and K. Esumi, *Bull. Chem. Soc. Jpn.*, **61** (1988) 341.
- [10] K. Meguro, T. Tano, K. Toigoe, H. Nakamura and K. Esumi, *Colloids Surf.*, **34** (1988) 381.
- [11] T. Tano, K. Esumi and K. Meguro, *J. Colloid Interface Sci.*, **133** (1989) 530.
- [12] J. Evans, *NATO ASI Ser. Ser. C (Surf. Organomet. Chem., Mol. Approaches Surf. Catal.)*, Vol. 231, Kluwer, Dordrecht, 1988, p. 47.
- [13] J. Evans, B. Hayden, F. Mosselmans and A. Murray, *J. Am. Chem. Soc.*, **114** (1992) 6912.
- [14] J. Evans, B. Hayden, F. Mosselmans and A. Murray, *Surf. Sci.*, **279** (1–2) (1992) 159.
- [15] B.T. Heaton, *Pure Appl. Chem.*, **60** (12) (1988) 1757.
- [16] A. Henglein, *J. Phys. Chem.*, **97** (1993) 5457.
- [17] K.J. Klabunde, Y.-X. Li and B.-J. Tan, *Chem. Mater.*, **3** (1991) 30.
- [18] K.J. Klabunde, *Science*, **224** (1984) 1329.
- [19] K.J. Klabunde and Y. Imizu, *J. Am. Chem. Soc.*, **106** (1984) 2721.
- [20] K.J. Klabunde and Y. Tanaka, *J. Mol. Catal.*, **21** (1983) 57.
- [21] H. Knözinger, in G. Paccioni, P.S. Bagus and F. Parmigiani (eds.), *Cluster Models for Surface and Bulk Phenomena*, Plenum, New York, 1992.
- [22] C. Larpent and H. Patin, *J. Mol. Catal.*, **44** (1988) 191.
- [23] L.N. Lewis, *Chem. Rev.*, **93** (1993) 2693.
- [24] L.N. Lewis and N. Lewis, *Chem. Mater.*, **1** (1989) 106.
- [25] L.N. Lewis and N. Lewis, *J. Am. Chem. Soc.*, **108** (1986) 7228.
- [26] L.N. Lewis, R. Uriarte and N. Lewis, *J. Catal.*, **127** (1991) 67.
- [27] T.A. Stromnova, I.N. Busygina, M.N. Vargaftik and I.I. Moiseev, *Metalloorg. Khim.*, **3** (1990) 803.
- [28] I.I. Moiseev, *Pure Appl. Chem.*, **61** (1989) 1755.
- [29] G. Schmid, *Endeavour*, **14** (1990) 172.
- [30] G. Schmid, *Aspects Homogen. Catal.*, **7** (1990) 1.
- [31] G. Schmid, H.A. Smit, M.P.J. van Staveren and R.C. Thiel, *New. J. Chem.*, **14** (1990) 559.
- [32] G. Schmid, N. Klein, B. Morun, A. Lehnert and J.O. Malm, *Pure Appl. Chem.*, **62** (1990) 559.
- [33] L.J. De Jongh, J.A.O. De Aguiar, H.B. Brom, G. Longoni, J.M. van Ruitenbeek, G. Schmid, H.A. Smit, M.P.J. van Staveren and R.C. Thiel, *Z. Phys. D.*, **12** (1989) 455.
- [34] N. Toshima and T. Takahashi, *Bull. Chem. Soc. Jpn.*, **65** (4) (1992) 400.
- [35] N. Toshima, M. Harada, T. Yonezawa, K. Kushihashi and K. Asakura, *J. Phys. Chem.*, **95** (1991) 7448.
- [36] N. Toshima, T. Takahashi and H. Hirai, *J. Macromol. Sci. Chem.*, **25** (5–7) (1988) 669.
- [37] N. Toshima, *J. Macromol. Sci. Chem.*, **27** (9–11) (1990) 1225.
- [38] B. Zhao and N. Toshima, *Chem. Express*, **5** (10) (1990) 721.
- [39] D.G. Duff, P.P. Edwards, J. Evans, J.T. Gauntlett and D.A. Jefferson, *Angew. Chem.*, **101** (1989) 610.
- [40] H.H. Lamb, B.C. Gates and H. Knözinger, *Angew. Chem.*, **100** (1988) 1162.
- [41] B.C. Gates, *Catalytic Chemistry*, Wiley, New York, 1993.
- [42] D. Brown, B.T. Heaton and J.A. Iggo, *Catal. Met. Complexes*, **12** (1991) 329.
- [43] R.W. Devenish, S. Mulley, B.T. Heaton and G. Longoni, *J. Mater. Res.*, **7** (10) (1992) 2810.
- [44] A. Henglein, P. Mulvaney, A. Holzwarth, T.E. Sosebee and A. Fojtik, *Ber. Bunsenges. Phys. Chem.*, **98** (1992) 754.
- [45] K. Matosuo and K.J. Klabunde, *J. Org. Chem.*, **47** (1982) 843.
- [46] K.J. Klabunde, S.C. Davis, H. Hattori and Y. Tanaka, *J. Catal.*, **54** (1978) 254.
- [47] K.J. Klabunde, H.F. Efnor, T.O. Murdock and R. Ropple, *J. Am. Chem. Soc.*, **98** (1976) 1021.
- [48] A.S. Berenblyum, A.G. Knizhnik, S.L. Mund and I.I. Moiseev, *J. Organomet. Chem.*, **234** (1982) 219.
- [49] M.N. Vargaftik, V.P. Zagorodnikov, I.P. Stolyarov, I.I. Moiseev, V.A. Likholobov, D.I. Kochubey, A.L. Churilin, V.I. Zaikovskiy, K.I. Zamaraev and G.I. Timofeeva, *J. Chem. Soc. Chem. Commun.*, (1985) 937.
- [50] I.I. Moiseev, T.A. Stromnova and M.N. Vargaftik, *J. Mol. Catal.*, **86** (1994) 71.
- [51] I.I. Moiseev, *Mekh. Katal. Novosibirsk*, **21** (1984) 72 (from Ref. Zh. Khim. (1985), Abstr. No. 4B4121).
- [52] I.I. Moiseev, *Itogi Nauki Tekh. Viniti. Kinet. Katal.*, **13** (1984) 147 (from Ref. Zh. Khim. (1984), Abstr. No. 16B4121).
- [53] G. Schmid, *Polyhedron*, **7** (1988) 2321.
- [54] G. Schmid, *Chem. Uns. Zeit.*, **22** (1988) 85.
- [55] G. Schmid, *Nachr. Chem., Tech. Lab.*, **35** (1987) 249.
- [56] G. Schmid, *Angew. Chem.*, **90** (1978) 417.
- [57] G. Schmid, *Struct. Bonding (Berlin)*, **62** (1985) 51.
- [58] H. Hirai, S. Komatsuzaki and N. Toshima, *Bull. Chem. Soc. Jpn.*, **57** (2) (1984) 488.

- [59] H. Hirai, H. Chawanya and N. Toshima, *Bull. Chem. Soc. Jpn.*, **58** (2) (1985) 682.
- [60] H. Hirai, S. Komatsuzaki and N. Toshima, *J. Macromol. Sci. Chem.*, **23** (8) (1986) 933.
- [61] N. Toshima, T. Teranishi and Y. Saito, *Makromol. Chem. Macromol. Symp.*, **59** (1992) 327.
- [62] C. Paal and C. Amberger, *Berichte*, **37** (1904) 124.
- [63] C. Paal and C. Amberger, *Berichte*, **38** (1905) 1398.
- [64] J.S. Bradley, in Ref. [1], pp. 464–471.
- [65] G. Schmid, *Chem. Rev.*, **92** (1992) 1709.
- [66] H. Liu and N. Toshima, *J. Chem. Soc. Chem. Commun.*, (1992) 1095.
- [67] J.S. Bradley, in Ref. [1], pp. 480–485.
- [68] J.S. Bradley, E.W. Hill, C. Klein, B. Chaudret and A. Duteil, *Chem. Mater.*, **5** (1993) 254.
- [69] K. Torigo and K. Esumi, *Langmuir*, **9** (1993) 1664.
- [70] J.H. Fendler, *Membrane—Mimetic Approach to Advanced Materials*, Springer, Berlin, 1994.
- [71] C. Larpent, F. Brisse-Le Menn and H. Patin, *Mol. Catal.*, **65** (1991) L35.
- [72] T. Sato, S. Kuroda, A. Takami, Y. Yonezawa and H. Hada, *Appl. Organomet. Chem.*, **5** (1991) 261.
- [73] T. Yonezawa, A. Takami, T. Sato, K. Yamamoto, T. Sasanuma, H. Ishida and A. Ishitani, *J. Appl. Phys.*, **68** (1990) 1297.
- [74] Y. Yonezawa, T. Sato, M. Ohno and H. Hada, *J. Chem. Soc. Faraday Trans. 1*, **83** (1987) 1559.
- [75] H. Hirai, Y. Nakao and N. Toshima, *Chem. Lett.*, **5** (1978) 545.
- [76] M. Ohtaki, M. Komiyama, H. Hirai and N. Toshima, *Macromolecules*, **24** (1991) 5567.
- [77] N. Toshima and T. Yonezawa, *Makromol. Chem. Macromol. Symp.*, **59** (1992) 281.
- [78] N. Toshima, M. Harada, Y. Yamazaki and K. Asakura, *J. Phys. Chem.*, **96** (1992) 9927.
- [79] H. Hirai, Y. Nakao and N. Toshima, *Chem. Lett.*, **9** (1976) 905.
- [80] N. Toshima, M. Ohtaki and T. Teranishi, *Reactive Polym.*, **15** (1991) 135.
- [81] G.V. Lischkin, A.Ya. Yuffa and V.Yu. Khinchagashvili, *Russ. J. Phys. Chem.*, **50** (1976) 1285.
- [82] J. Kiwi and M. Grätzel, *J. Am. Chem. Soc.*, **101** (1979) 7214.
- [83] H. Bönemann, W. Brijoux, R. Brinkmann, R. Fretzen, Th. Joußen, R. Köppler, B. Korall, P. Neiteler and J. Richter, *J. Mol. Catal.*, **86** (1994) 129.
- [84] H. Bönemann, W. Brijoux, R. Brinkmann, E. Dinjus, R. Fretzen, Th. Joußen and B. Korall, *J. Mol. Catal.*, **74** (1992) 323.
- [85] H. Bönemann, R. Brinkmann, R. Köppler, P. Neiteler and J. Richter, *J. Adv. Mater.*, **4** (1992) 804.
- [86] H. Bönemann, W. Brijoux, R. Brinkmann, E. Dinjus, R. Fretzen and B. Korall, German Patent DE 4 111 719, 1991 (to Studiengesellschaft Kohle mbH).
- [87] H. Bönemann, R. Brinkmann and P. Neiteler, *Appl. Organomet. Chem.*, **8** (1994) 361.
- [88] H. Bönemann and W. Brijoux, in K.E. Gonsalves, G.-M. Chow, T.D. Xiao and R.C. Cammarata (eds.), *Molecularly Designed Ultrafine Nanostructured Materials*, Vol. 351, from the MRS Symp. Proc. Ser., 1994
- [89] H. Bönemann and W. Brijoux, in A. Fürstner (ed.), *Active Metals*, VCH, Weinheim, 1995, p. 339.
- [90] L.E. Aleandri, H. Bönemann, D.J. Jones, J. Richter and J. Rozière, submitted to *J. Mater. Chem.*
- [91] H. Bönemann, W. Brijoux, J. Richter, R. Becker, J. Hornes and J. Rothe, *Z. Naturforsch. Teil B*, **50** (1995) 333.
- [92] M.T. Reetz and W. Helbig, *J. Am. Chem. Soc.*, **116** (1994) 7401.
- [93] M.T. Reetz, W. Helbig, S. Quaiser, U. Stimmig, N. Breuer and R. Vogel, *Science*, **267** (1995) 367.
- [94] M.T. Reetz and S. Quaiser, *Angew. Chem.*, **107** (1995) 2461.
- [95] H. Bönemann and B. Korall, *Angew. Chem.*, **104** (1992) 1506.
- [96] H. Bönemann, W. Brijoux, Th. Hindenburg, R. Franke, J. Hornes, J. Pollmann and J. Rothe, submitted to *J. Am. Chem. Soc.*
- [97] H. Bönemann, W. Brijoux and Th. Joussen, *Angew. Chem.*, **102** (1990) 324; *Angew. Chem. Int. Ed. Engl.*, **29** (1990) 273.
- [98] H. Bönemann, W. Brijoux, R. Brinkmann, E. Dinjus, Th. Joußen and B. Korall, *Angew. Chem.*, **103** (1991) 1344; *Angew. Chem. Int. Ed. Engl.*, **30** (1991) 1312.
- [99] R. Köppler, *Ph.D. Thesis*, University of Aachen, 1995, pp. 58–64.
- [100] Th. Hindenburg, *Ph.D. Thesis*, University of Aachen, 1995.
- [101] Ref. [99], pp. 65–67.
- [102] H. Bönemann, W. Brijoux and J. Richter, unpublished results, 1992.
- [103] H. Bönemann, W. Brijoux, J. Richter, K. Siepen, R. Franke, J. Hornes, J. Pollmann and J. Rothe, submitted to *Fresenius J. Anal. Chem.*
- [104] U. Simon, G. Schön and G. Schmid, *Angew. Chem. Int. Ed.*, **32** (1993) 250.
- [105] R.J. Behm, G. Witek, M. Noeske, G. Mestl, Sh. Shaikhutdinov, submitted to *Catal. Lett.*
- [106] N. Egeler, *Ph.D. Thesis*, University of Aachen, 1992.
- [107] A. Schulze Tilling, *Ph.D. Thesis*, University of Aachen, in preparation.
- [108] C. Brönnimann T. Mallat and A. Baiker, *J. Chem. Soc. Chem. Commun.*, (1995) 1377.
- [109] Kao Corporation, EP 0 142 725 (Prior. 24.10.1983).
- [110] Degussa AG, EP 0 350 741 B 1 (Prior. 09.07.1988).
- [111] K. Siepen, *Ph.D. Thesis*, University of Aachen, in preparation.
- [112] G. Braun, *Ph.D. Thesis*, University of Aachen, in preparation.
- [113] Y. Orito, S. Inai and S. Niwa, *J. Chem. Soc. Jpn.*, (1979) 1118.
- [114] H.U. Blaser, H.P. Jalett, D.M. Monti, J.F. Reber and J.T. Welnli, *Stud. Surf. Sci. Catal.*, **59** (1988) 153.
- [115] J.T. Welnli, A. Baiker, D.M. Monti and H.U. Blaser, *J. Mol. Catal.*, **61** (1990) 207.
- [116] U.K. Singh, R.N. Landau, Y. Sun, C. LeBlond, D.G. Blackmond, S.K. Tanielyan and R.L. Augustine, *J. Catal.*, **154** (1995) 91.
- [117] J.S. Bradley, J.M. Millar, E.W. Hill, C. Klein, B. Chaudret and A. Duteil, *Proc. 10th Int. Congress on Catalysis, Budapest, Hungary, July 19–24, 1992*.
- [118] J.S. Bradley, E.W. Hill, B. Chaudret and A. Duteil, *Langmuir*, **11** (1995) 693.
- [119] F. Solymosi and M. Pasztor, *J. Phys. Chem.*, **89** (1985) 4789.
- [120] M. Primet, *J. Chem. Soc. Faraday Trans. 1*, **74** (1978) 2570.
- [121] M. Baerns and S. Trautmann, *J. Catal.*, **150** (1994) 335.